Energy Storage Materials 24 (2020) 291–296

Contents lists available at ScienceDirect

Energy Storage Materials

journal homepage: www.elsevier.com/locate/ensm

Highly stable Ni-rich layered oxide cathode enabled by a thick protective layer with bio-tissue structure

Yujing Bi [a,b,c], Meng Liu [b], Biwei Xiao [c], Yang Jiang [b], Huan Lin [b], Zhenggang Zhang [b], Guoxin Chen [b], Qian Sun [c], Haiyong He [b], Feng Huang [b], Xueliang Sun [c,***], Deyu Wang [b,d,**], Ji-Guang Zhang [a,*]

[a] Pacific Northwest National Laboratory, Richland, WA, 99354, USA
[b] Ningbo Institute of Materials Technology and Engineering, Chinese Academy of Sciences, Ningbo, 315201, China
[c] Department of Mechanical and Materials Engineering, University of Western Ontario, London, ON, N6A 5B9, Canada
[d] Tianmu Lake Institute of Advanced Energy Storage Technology, Liyang, 213300, China

ARTICLE INFO

Keywords:
Protective layer
Nickel rich
Lithium ion batteries
Bio-tissue structure
Safety

ABSTRACT

Ni-rich layered oxide ($LiNi_xMn_yCo_zO_2$ (NMC), $x > 60\%$), one of the most promising cathode materials for high-energy lithium ion batteries (LIBs), still suffers from surface instability even with the state-of-art protective coatings, which normally are limited to ≤10 nm to maintain the required kinetics. Here we demonstrate a highly conductive protective layer with bio-tissue structure that can enable high-rate operation of NMC cathodes even with a thickness exceeding 40 nm. With this thick protection layer, the modified $LiNi_{0.8}Mn_{0.1}Co_{0.1}O_2$ (NMC811) cathode retains 90.1% and 88.3% of its initial capacity after 1000 cycles in coin cells and pouch cells, respectively. This novel membrane is composed of crystalline nano-domains surrounded by ~1 nm amorphous phase, which is an effective distance to enable tunneling of electrons and Li^+ ions between these domains. The coated NMC811 cathode releases ~55.3% less heat under thermal abuse and largely enhances his safety feature during puncture test. The coating also enables excellent electrochemical stability of NMC811 even after it was exposed to a moist environment for four weeks at 55 °C, which is critical for large-scale production of high-energy-density LIBs.

Nickel (Ni)-rich layered materials ($LiNi_xMn_yCo_zO_2$ (NMC), $x > 60\%$) are a very promising cathode for high-energy-density lithium (Li) ion batteries (LIBs), especially for high-power batteries. An appropriate interphase between electrode and electrolyte plays a crucial role in the electrochemical performance of LIBs [1–4]. In recent years, various surface treatment methods have been developed to improve the interphase compatibility in LIBs [5–7]. For example, carbon coating was used to activate the insulating $LiFePO_4$ [8–10], and modified ceramic layers were used to stabilize the Li-transition metal oxide cathodes to improve their cycle life and safety [11–14]. Various coating materials, such as oxides [15–26], phosphates [27–30], fluorides [31–34], and even conductive polymers have also been used to stabilize the NMC/electrolyte interphase in recent years [35–38]; however, these coatings are still inadequate to provide the necessary safety and cycling stability to Ni-rich cathodes for their practical application [39]. As is known, to sustain acceptable kinetics, these monophase crystalline/amorphous layers are controlled to less than 10 nm thick, since the coating materials are electronic and/or ionic insulators [40], but such a thin coating may also lead to nonuniform coverage/protection of particles. Therefore, Ni-rich cathodes may require a thicker modified layer with low impedance to enhance the protection of Ni-rich NMC cathodes.

Recently, manganese (Mn)-rich gradient materials were proposed to improve the stability of Ni-rich cathodes [41–45]. However, the Mn-rich surface is not favored in industry because exposed Mn cations will be dissolved into the electrolytes as Mn^{2+} cations, which could deposit on graphite and greatly increase the interfacial polarization [46,47]. A surface-cobalt (Co)-rich design degrades the electrochemical performance of Ni-rich materials, as shown in this work, although it possess a relatively stable surface. Therefore, an effective protective strategy to improve the comprehensive performance of Ni-rich materials is still

* Corresponding author.
** Corresponding author. Ningbo Institute of Materials Technology and Engineering, Chinese Academy of Sciences, Ningbo, 315201, China.
*** Corresponding author.
E-mail addresses: xsun9@uwo.ca (X. Sun), wangdy@nimte.ac.cn (D. Wang), jiguang.zhang@pnnl.gov (J.-G. Zhang).

https://doi.org/10.1016/j.ensm.2019.08.006
Received 10 February 2019; Received in revised form 29 July 2019; Accepted 5 August 2019
Available online 9 August 2019

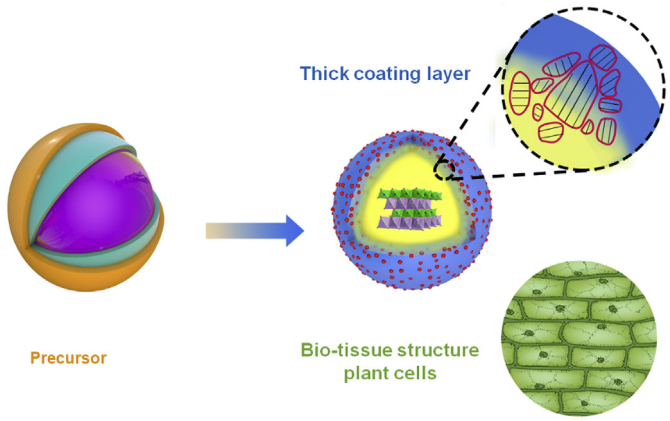

Scheme 1. Schematic of core–medial-shell structure precursor and Ni-rich cathode coated with a thick, bio-tissue-like layer after high-temperature calcination.

lacking.

In this work, we report the successful development of a 40–50 nm thick modified layer, ~5 times thicker than the state-of-art coating layers, to address the surface sensitivity of $LiNi_{0.8}Mn_{0.1}Co_{0.1}O_2$ without significantly reducing its rate capability. This thick membrane possesses a bio-tissue structure, in which the crystalline layered-oxide nano-domains are scattered in the amorphous species less than 1 nm apart, like cells surrounded by interstitials in plant tissue, as shown in Scheme 1. These nanocrystalline islands could transport both electrons and Li^+ ions through the thick membrane via quantum tunneling. Protected by this surface structure, the modified $LiNi_{0.8}Mn_{0.1}Co_{0.1}O_2$ presents excellent electrochemical performance during cycling, thermal abuse, and moisture exposure, indicating its promising potential for LIBs, especially to power electric vehicles.

The as-prepared samples are a pure layered oxide that can be attributed to the R-3m group of the hexagonal crystal family, as shown in Fig. S1 and Table S1. Both *a*-axis and *c*-axis lengths are close to those of pure $LiNi_{0.8}Mn_{0.1}Co_{0.1}O_2$ and larger than those of the Co-rich-gradient sample, which was obtained from the core-shell–structured precursor of $Ni_{0.8}Mn_{0.1}Co_{0.1}(OH)_2-0.1Co(OH)_2$. Since the Co^{3+} ionic radius is smaller than that of Ni^{3+}, increasing the Co ratio in the gradient sample will lead to lattice shrinkage, as shown in the lattice volume comparison in Table S1. The lattice parameters of our coated sample are different from those of the Co-gradient sample, indicating that the Co cations are not uniformly distributed.

As shown in Fig. 1, the sintered particles are covered by a thick shell layer without an interlayer, although the core–medial-shell structure is clearly identified in the precursors (Fig. S2). This shell layer is 40–50 nm thick, ~5 times thicker than the rough coating layer used in other work [25,40,48]. High-resolution transmission electron microscopy (HRTEM) was used to examine the structure in detail. This thick layer is mainly composed of crystalline nano-domains with diameters of 2–20 nm separated by an amorphous phase with gaps smaller than 1 nm, which is the effective length of quantum tunneling. When zirconium grows with a high concentration of Co, it will not form a solid solution with layered oxide cathode materials, even at high temperature, because of their lattice difference [49]. In this condition, the lithium-zirconium-oxygen (Li–Zr–O, Fig. S3) interlayer is designed to impede diffusion of the outermost Co to the core material and create a gradient structure in the thick surface region. The nano-domains with layered structure were scattered in the region of zirconium compounds. Disturbed by layered structure phase during calcination, Li–Zr–O phase exists as amorphous phase after synthesis. This distribution is similar with that of plant tissues, where the plant cells are scattered among the interstitials. This is the first time the bio-tissue structure has been observed in LIB materials, to the best of our knowledge.

It is interesting to note that the crystalline domains in this thick shell layer vary slightly from the outermost surface to the bulk. In selected regions, the space between the crystalline planes changes along the radial direction from 0.200 nm to 0.202 nm–0.204 nm, which should correspond to the (104) plane of $LiNi_{1-x-y}Mn_xCo_yO_2$. Fast Fourier transform (FFT) and inverse-FFT images that filtered the noisy background are used to compare the crystal spacing, as shown in Fig. S4. This variation indicates that the Ni ratio gradually increases in the outward radial direction. In contrast, lattice fringes of pristine and Co-rich gradient samples are uniform, which means that they are continuously crystalline

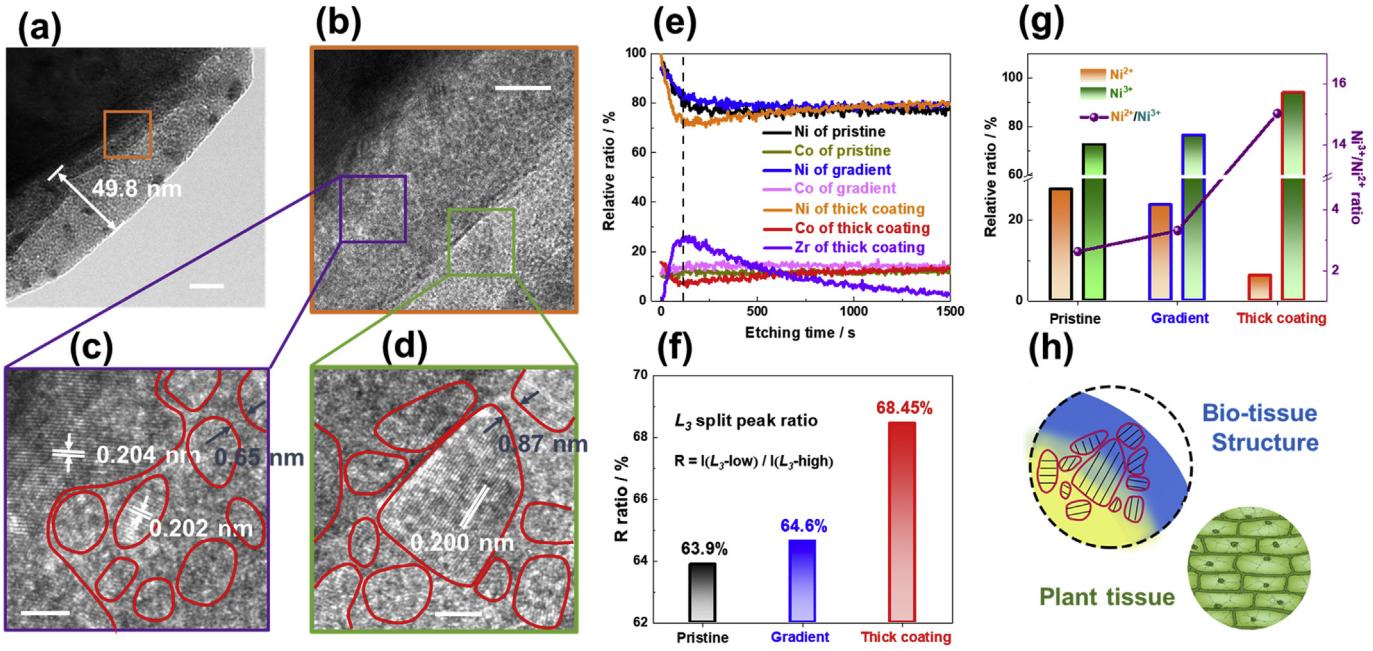

Fig. 1. Physical characterizations of our designed materials: (a–d) TEM and HRTEM images of thickly coated $LiNi_{0.8}Mn_{0.1}Co_{0.1}O_2$; (e) Elemental depth profiles tested via SIMS; (f) Ni^{2+} and Ni^{3+} ratios out of total Ni fitted by XPS results; (g) Ni L_3 split peak ratio calculated from Ni *L*-edge soft XAS spectra. (h) Schematic for comparison of prepared material structure with plant tissue structure.Scale bar in (a) is 20 nm. Scale bar in (b) is 10 nm. Scale bars in (c) and (d) are 2 nm.

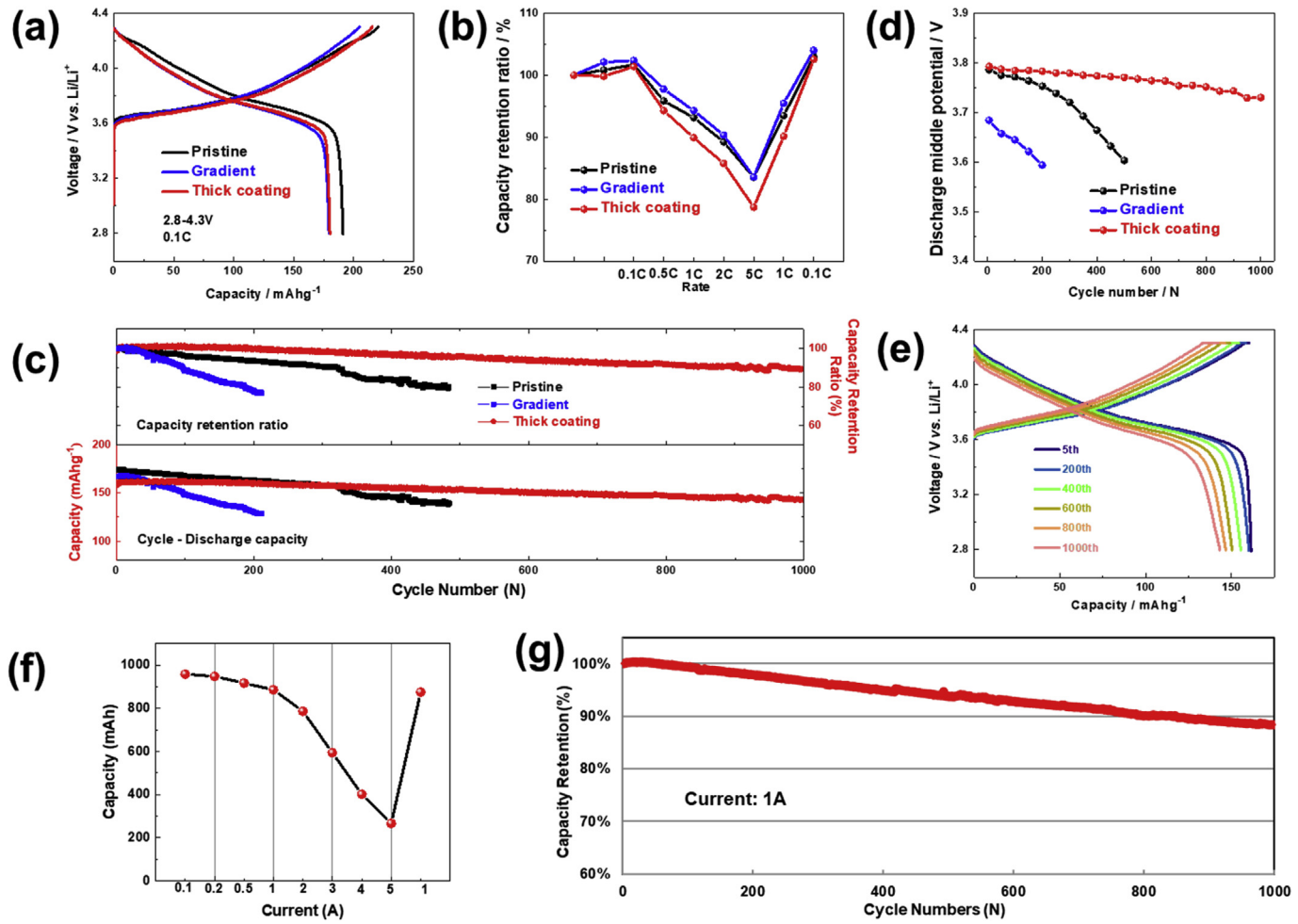

Fig. 2. Electrochemical performance of the investigated samples. (a) Initial charge and discharge curves at 0.1 C rate. (b) Comparison of rate capacity retention. (c) Cycling stability and coulombic efficiency at 1 C rate in coin cell. (d) Midpoint discharge voltage during 1 C cycle. (e) Charge and discharge curves of thick coating material at specific cycles. (f) Rate capability of 1 Ah pouch cell using cathode material with bio-tissue structure (graphite as anode). (g) Cycling performance of 1 Ah pouch cell between 2.8-4.2 V using 1 A current.

without phase separation, as shown in Fig. S5.

Radial distribution of the elements was analyzed by secondary ion mass spectroscopy (SIMS) along the radial direction with Ar^+ ion etching. As shown in Fig. 1e, the ratio of zirconium initially increased rapidly with longer etching time, and peaked at the depth corresponding to 160 s etching, which is approximately ~5 nm [50,51]. After the peak, the zirconium ratio slowly diminished throughout the tested depth and was still detectable after etching for 1500 s. This phenomenon can be attributed to the three-dimensional distribution of zirconia in the shell layer.

As for other elements, the gradient sample possesses the highest Co concentration and lowest Ni ratio on the surface when compared to the control samples. It demonstrates that our designed sample has a Co- and Zr-rich surface, which should be much more stable than one depleted of Co and Zr. Furthermore, the results obtained from x-ray diffraction (XRD) and HRTEM data indicate the Co cations are mainly concentrated in the thick coating layer and surrounded by amorphous regions, which exert a negligible influence on the XRD pattern, as confirmed by the energy dispersive spectroscopy results in Fig. S6.

X-ray photoelectron spectroscopy (XPS) was used to characterize the surface chemical environment and composition within 2–3 nm depth. As shown in Fig. S7 and Table S2, zirconium accounts for a fraction of 15.89% among the total metal ions, confirming the surface richness of zirconium in our designed sample. Furthermore, the Ni content is obviously reduced to 52.04 at%, much lower than the pristine and gradient samples, indicating the effectiveness of coating in lowering surface Ni content. Based on the XPS data, the fractions of Ni^{2+} out of the total Ni are 27.53, 23.68, and 6.24 at% for pristine, gradient, and our designed samples, respectively, as shown in Fig. 1f and Table S3. According to previous work indicating that Ni-rich cathodes would generate Ni^{2+} cations via decomposition in ambient conditions [52,53], our designed sample should possess a much better chemical stability in a moist atmosphere.

Soft x-ray absorption spectroscopy (XAS) was employed to analyze the Ni at the depth of ~5 nm in total electron yield (TEY) mode, and of ~100 nm in fluorescence yield (FY) mode [39,54]. As shown in Fig. 1f–g and Fig. S8, the Ni *L*-edge L_3 peak splits into L_3-high at 861.4 eV and L_3-low at 863.3 eV, which correspond to Ni^{2+} and Ni^{3+}, respectively [55, 56]. The sample with the thick-layer coating presents the highest value of L_3-high/L_3-low, namely Ni^{3+}/Ni^{2+}, in TEY mode. This further confirms that the protective layer suppresses the surface decomposition of the Ni-rich cathode, which is consistent with XPS results. The Ni^{3+}/Ni^{2+} values are almost the same for all three samples in FY mode, demonstrating their similarity in the domain around 100 nm depth. This further reveals that our protective layer only changes the surface chemistry and structure of the Ni-rich cathode.

To investigate the effect of a thick coating layer (~15 times thicker than the typical coatings) on Ni-rich cathode material, we compared the electrochemical performance of our coated samples with those of pristine and gradient materials. As shown in Fig. 2b, at 0.1 C rate, the coated

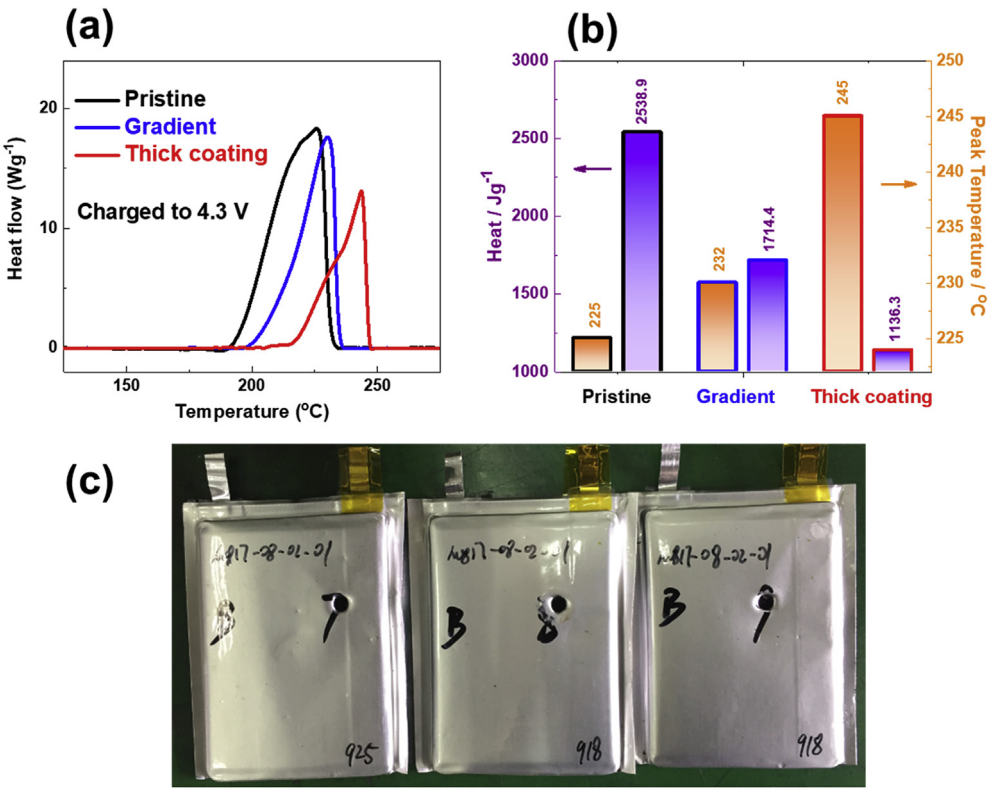

Fig. 3. Thermal analysis of the investigated samples: (a) Differential scanning calorimetry profiles of the delithiated Ni-rich cathodes in a 4.3 V charged state with electrolyte; (b) Comparison of exothermic peaks and heat release values; (c) Photos of 1 Ah pouch cell punctured by stainless steel nail.

sample exhibits a discharge capacity as high as ~182 mAh g^{-1}, which is similar to that of the gradient sample and lower than that of the pristine $LiNi_{0.8}Mn_{0.1}Co_{0.1}O_2$ (193 mAh g^{-1}). At 0.5 C and higher rates, the coated samples exhibit only 5–10% lower capability (see Fig. S9) than those of the control samples. The good kinetics of the thickly coated samples can be attributed to its bio-tissue structure in the thick shell layer. We notice that the crystalline domains are separated by less than 1 nm, which is the effective distance of quantum tunneling [57]. Therefore, the charge carriers could travel through the ternary-oxide crystalline nano-domain, hop to an adjacent nano-domain via quantum tunneling, and then diffuse into the bulk. Clearly, our approach satisfies the need to construct a better protective layer on cathode materials without significantly sacrificing the rate capability of cathode materials.

The cyclic performance of the samples was tested at 0.5 C charge and 1 C discharge between ~2.8 and ~4.3 V *vs.* Li/Li^+. Our designed sample presents excellent cyclic stability, with 90.1% of the initial discharge capacity remaining in the 1000th cycle (Fig. 2c). As shown in Fig. 2d and e, its discharge midpoint potential gradually decreases from 3.80 V *vs.* Li^+/Li at the initial cycle to 3.71 V *vs.* Li/Li^+ at the 1000th cycle, and even its charge-discharge curve in the 1000th cycle retains the typical characteristics of layered ternary oxides. In contrast, the pristine and the gradient samples retain 80% of their initial capacities in the 484th cycle and 211th cycle, respectively.

Electrochemical and safety performance was also evaluated using pouch cell (graphite was used as anode). As shown in Fig. 2f and g, the pouch cell retained 88.3% of its initial capacity after 1000 cycles, which is similar with the retention ratio in coin cell using Li metal as anode (90.1%). Long cycling life obtained in both coin cell and pouch cell confirms that bio-tissue structure could significantly enhances the cycling stability of nickel rich cathode. The designed 1 Ah pouch cell could deliver 88.6%, 78.6%, 59.4%, 40.1% and 26.6% capacity at 1, 2, 3, 4, 5 A current, respectively. Considering the current loading ability for EV charging, 78.6% capacity retention ratio at 2C (corresponding to 2 A for 1 Ah pouch cell) in full cell could meet the requirement for high energy density batteries.

To further illustrate the protective effect of this thick layer, the cycled electrodes of the investigated samples were evaluated after being disassembled in the glove box; scanning electron microscope (SEM) images are shown in Fig. S10. The crystalline phase of thick-coating and Co-gradient samples remains intact after cycling, as does that of the pristine sample (Fig. S11). Diffraction peaks of cycled pristine electrode at a 2θ of 43.1° and 47.3° correspond to NiO-like phase; this is consistent with references that indicate Ni-rich material easily generates NiO-like phase on the surface during degradation [50,58–60]. Particles of the pristine and gradient samples were covered with some extra substances, and the electrolyte had dried up in both systems. These results indicate that quick consumption of the electrolytes is the reason for capacity fading in both systems. As for the sample with the ultra-thick protective layer, the particles are almost as smooth as the pristine condition after 1000 cycles. Unlike the pristine materials in Fig. S10, most of the thickly coated Ni-rich particles are uncracked even after 1000 cycles. It is believed that the bio-tissue structure with nano-domains in amorphous regions contributed to releasing micro-strain and suppressing particle cracking [61–63].

Thermal stability has been one of the crucial concerns for Ni-rich cathodes since they were invented in the 1980s. The side reactions between cathodes and electrolyte would generate a huge amount of heat and induce catastrophic accidents in the full batteries during thermal abuse. Our thick protective layer significantly improves the thermal stability of Ni-rich materials, as shown in Fig. 3. The exothermal reaction for our designed sample began at 215 °C and peaked at 245 °C with a total heat of 1136.3 J g^{-1}; the released heat is much lower than those of the pristine (188 °C, 225 °C, and 2538.9 Jg^{-1}) and Co-gradient sample (196 °C, 232 °C, 1714.4 Jg^{-1}). This thick coating layer reduces the released heat to 44.1% of the pristine and postpones the exothermic reaction by ~20 °C. Furthermore, this thermal behavior is close to that of $LiNi_{0.5}Co_{0.3}Mn_{0.2}O_2$ [64], indicating our approach changes the Ni-rich material to a safer cathode. It is well known that puncture safety test is

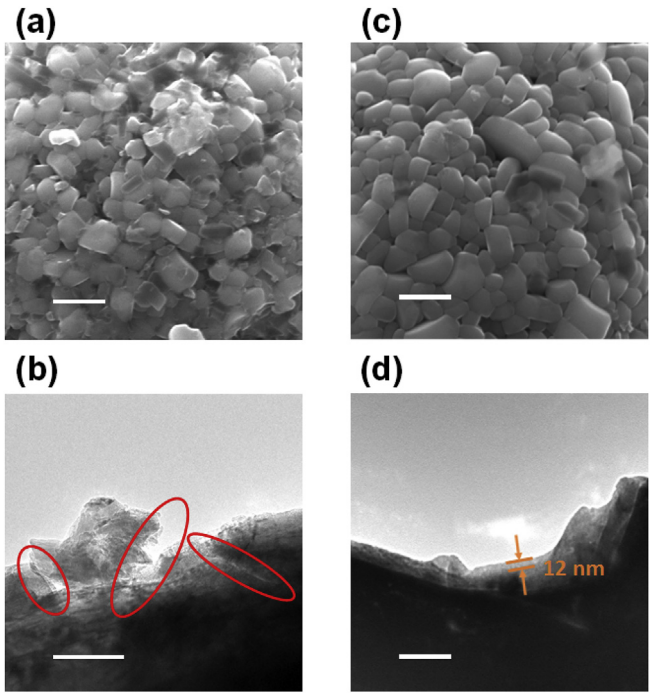

Fig. 4. SEM and TEM images of pristine and thickly coated, Ni-rich material after being stored in a 55 °C moist stream for four weeks: (a), (b) pristine $LiNi_{0.8}Mn_{0.1}Co_{0.1}O_2$; (c), (d) thickly coated $LiNi_{0.8}Mn_{0.1}Co_{0.1}O_2$. Scale bars in (a) and (c) are 1 μm. Scale bars in (b) and (d) are 100 nm.

one of the most rigorous tests for nickel rich cathode pouch cells. Protected by a bio-tissue structure, pouch cells using thick coated nickel rich cathode present high endurance in puncture safety test. As shown in Fig. 3c, fire or explosion was not observed during pouch cell punctured by stainless steel nail. The pouch cell appearance does not change much after puncture test. Due to excellent protection of thick bio-tissue like interphase, surface sensitivity of Ni rich NMC cathode is passivated and battery safety is largely enhanced and results in the much enhanced safety for high energy density battery.

Moisture sensitivity is another key challenge for Ni-rich materials [65,66]. To minimize the detrimental effect of humidity, industry must use an expensive dry-room atmosphere, from slurry mixing to electrolyte injection, to produce batteries. To investigate the effect of our thick coating layer against moisture exposure, the samples were placed in a ⌀380 mm desiccator with 200 mL water and stored at 55 °C for four weeks. As shown in Fig. 4, the pristine $LiNi_{0.8}Mn_{0.1}Co_{0.1}O_2$ particles are coated by a ~200 nm thick layer of decomposed substances and even form some cracks after being stored in such a humid environment, indicating its severe decomposition under this condition. In contrast, the thickly coated sample retains a much neater exterior. The surface layer has only grown to 10–15 nm after storage in the humid environment. After extensive exposure to humidity, our coated sample presents higher discharge capacity, 179.2 mAh g^{-1}, only 2.8 mAh g^{-1} lower than the material not exposed to moisture, as shown in Fig. S12a. It also exhibits the better cycling stability, still retaining 82% capacity after 200 cycles, whereas the pristine and gradient samples only retain 37% and 60% (compared in Fig. S12b). Obviously, the protective layer developed in this work significantly improves the stability under humidity.

In summary, we have developed a novel strategy to construct a 40–50-nm-thick shell layer with bio-tissue structure on $LiNi_{0.8}Mn_{0.1}Co_{0.1}O_2$ particles to stabilize their sensitive surface without greatly reducing the kinetics. The acceptable rate capability of our designed sample is related to the structural stability of this layer, which is composed of crystalline domains separated by less than 1 nm. It is probable that the carriers move through the ternary-oxide crystalline domain, hop to an adjacent domain via quantum tunneling, and then diffuse into the bulk. Our approach fills the need to construct a thick protective layer on cathode particles without significantly decreasing their rate capability. With the protection of this thick layer, our coated samples presented excellent stability under the long-term cycling test, thermal abuse, and moisture exposure. Therefore, this approach could largely facilitate large-scale manufacturing and safe storage of Ni-rich cathodes for high-energy LIBs.

Acknowledgment

This work was supported by the National Natural Science Foundation of China (Grant No. 51572273), the “Strategic Priority Research Program” (Grant No. XDA09010403). J-G. Z is supported by the Assistant Secretary for Energy Efficiency and Renewable Energy, Office of Vehicle Technologies, Advanced Battery Materials Research (BMR) program of the U.S. Department of Energy.

Appendix A. Supplementary data

Supplementary data to this article can be found online at https://doi.org/10.1016/j.ensm.2019.08.006.

References

[1] M. Armand, J.-M. Tarascon, Building better batteries, Nature 451 (2008) 652–657.
[2] K. Wang, X. Li, J. Chen, Surface and interface engineering of electrode materials for lithium-ion batteries, Adv. Mater. 27 (2014) 527–545.
[3] P. Yan, J. Zheng, Z. Wang, G. Teng, S. Kuppan, J. Xiao, G. Chen, F. Pan, J.-G. Zhang, C.-M. Wang, Ni and Co segregations on selective surface facets and rational design of layered lithium transition-metal oxide cathodes, Adv. Energy Mater. 6 (2016) 1502455.
[4] Y. Ding, Z.P. Cano, A. Yu, J. Lu, Z. Chen, Automotive Li-ion batteries: current status and future perspectives, Electrochem. Energy Rev. 2 (2019) 1–28.
[5] J. Lu, Z. Chen, Z. Ma, F. Pan, L.A. Curtiss, K. Amine, The role of nanotechnology in the development of battery materials for electric vehicles, Nat. Nanotechnol. 11 (2016) 1031–1038.
[6] J.-M. Tarascon, M. Armand, Issues and challenges facing rechargeable lithium batteries, Nature 414 (2001) 359–367.
[7] B. Dunn, H. Kamath, J.-M. Tarascon, Electrical energy storage for the grid: a battery of choices, Science 334 (2011) 928–935.
[8] J.D. Wilcox, M.M. Doeff, M. Marcinek, R. Kostecki, Factors influencing the quality of carbon coatings on $LiFePO_4$, J. Electrochem. Soc. 154 (2007) A389.
[9] J. Wang, J. Yang, Y. Tang, J. Liu, Y. Zhang, G. Liang, M. Gauthier, Y.C. Chen-Wiegart, M. Norouzi Banis, X. Li, R. Li, J. Wang, T.K. Sham, X. Sun, Size-dependent surface phase change of lithium iron phosphate during carbon coating, Nat. Commun. 5 (2014) 3415.
[10] L. Guo, Y. Zhang, J. Wang, L. Ma, S. Ma, E. Wang, Y. Bi, D. Wang, W.C. McKee, Y. Xu, J. Chen, Q. Zhang, C. Nan, L. Gu, P.G. Bruce, Z. Peng, Unlocking the energy capabilities of micron-sized $LiFePO_4$, Nat. Commun. 6 (2015) 7898.
[11] W. Liu, P. Oh, X. Liu, M.J. Lee, W. Cho, S. Chae, Y. Kim, J. Cho, Nickel-rich layered lithium transition-metal oxide for high-energy lithium-ion batteries, Angew. Chem. Int. Ed. 54 (2015) 4440–4457.
[12] A.M. Wise, C. Ban, J.N. Weker, S. Misra, A.S. Cavanagh, Z. Wu, Z. Li, M.S. Whittingham, K. Xu, S.M. George, M.F. Toney, Effect of Al_2O_3 coating on stabilizing $LiNi_{0.4}Mn_{0.4}Co_{0.2}O_2$ cathodes, Chem. Mater. 27 (2015) 6146–6154.
[13] A. Kraytsberg, Y. Ein-Eli, Conveying advanced Li-ion battery materials into practice the impact of electrode slurry preparation skills, Adv. Energy Mater. 6 (2016) 1600655.
[14] X. Yu, A. Manthiram, Electrode–electrolyte interfaces in lithium-based batteries, Energy Environ. Sci. 11 (2018) 527–543.
[15] J.W. Choi, D. Aurbach, Promise and reality of post-lithium-ion batteries with high energy densities, Nat. Rev. Mater. 1 (2016) 16013.
[16] W. Li, B. Song, A. Manthiram, High-voltage positive electrode materials for lithium-ion batteries, Chem. Soc. Rev. 46 (2017) 3006–3059.
[17] A. Manthiram, J.C. Knight, S.-T. Myung, S.-M. Oh, Y.-K. Sun, Nickel-rich and lithium-rich layered oxide cathodes: progress and perspectives, Adv. Energy Mater. 6 (2016) 1501010.
[18] A. Manthiram, B. Song, W. Li, A perspective on nickel-rich layered oxide cathodes for lithium-ion batteries, Energy Storage Mater. 6 (2017) 125–139.
[19] D. Aurbach, K. Gamolsky, B. Markovsky, G. Salitra, Y. Gofer, U. Heider, R. Oesten, M. Schmidt, The study of surface phenomena related to electrochemical lithium intercalation into Li_xMO_y host materials (M = Ni, Mn), J. Electroanal. Chem. 147 (2000) 1322–1331.
[20] J. Cho, T.-J. Kim, Y.J. Kim, B. Park, High-performance ZrO_2 coated $LiNiO_2$ cathode material, Electrochem. Solid State Lett. 4 (2001) A159–A161.

[21] N. Taguchi, H. Sakaebe, T. Akita, K. Tatsumi, Z. Ogumi, Characterization of surface of $LiCoO_2$ modified by Zr oxides using analytical transmission electron microscopy, J. Electrochem. Soc. 161 (2014) A1521–A1526.

[22] J. Zhang, Z. Li, R. Gao, Z. Hu, X. Liu, High rate capability and excellent thermal stability of Li^+-Conductive Li_2ZrO_3-coated $LiNi_{1/3}Co_{1/3}Mn_{1/3}O_2$ via a synchronous lithiation strategy, J. Phys. Chem. C 119 (2015) 20350–20356.

[23] X. Li, J. Liu, M.N. Banis, A. Lushington, R. Li, M. Cai, X. Sun, Atomic layer deposition of solid-state electrolyte coated cathode materials with superior high-voltage cycling behavior for lithium ion battery application, Energy Environ. Sci. 7 (2014) 768–778.

[24] Y. Su, S. Cui, Z. Zhuo, W. Yang, X. Wang, F. Pan F, Enhancing the high-voltage cycling performance of $LiNi_{0.5}Mn_{0.3}Co_{0.2}O_2$ by retarding its interfacial reaction with an electrolyte by atomic-layer-deposited Al_2O_3, ACS Appl. Mater. Interfaces 7 (2015) 25105–25112.

[25] S.-T. Myung, K. Izumi, S. Komaba, Y.-K. Sun, H. Yashiro, N. Kumagai, Role of alumina coating on Li-Ni-Co-Mn-O particle as positive electrode material for lithium-ion batteries, Chem. Mater. 17 (2005) 3695–3704.

[26] W.-S. Yoon, K.-W. Nam, D. Jang, K.Y. Chung, J. Hanson, J.-M. Chen, X.-Q. Yang, Structural study of the coating effect on the thermal stability of charged MgO-coated $LiNi_{0.8}Co_{0.2}O_2$ cathodes investigated by in situ XRD, J. Power Sources 217 (2012) 128–134.

[27] C.-H. Jo, D.-H. Cho, H.-J. Noh, H. Yashiro, Y.-K. Sun, S.T. Myung, An effective method to reduce residual lithium compounds on Ni-rich $Li[Ni_{0.6}Co_{0.2}Mn_{0.2}]O_2$ active material using a phosphoric acid derived Li_3PO_4 nanolayer, Nano Res. 8 (2014) 1464–1479.

[28] K. Park, J.-H. Park, S.-G. Hong, B. Choi, S.-W. Seo, J.-H. Park, K. Min, Enhancement in the electrochemical performance of zirconium/phosphate Bi-functional coatings on $LiNi_{0.8}Co_{0.15}Mn_{0.05}O_2$ by the removal of Li residuals, Phys. Chem. Chem. Phys. 18 (2016) 29076–29085.

[29] K. Tan, M. Reddy, G. Rao, B. Chowdari, Effect of $AlPO_4$-coating on cathodic behaviour of $Li(Ni_{0.8}Co_{0.2})O_2$, J. Power Sources 141 (2005) 129–142.

[30] G.-R. Hu, X.-R. Deng, Z.-D. Peng, K. Du, Comparison of $AlPO_4$- and $Co_3(PO_4)_2$-coated $LiNi_{0.8}Co_{0.2}O_2$ cathode materials for Li-ion battery, Electrochim. Acta 53 (2008) 2567–2573.

[31] P. Yue, Z. Wang, H. Guo, X. Xiong, X. Li, A low temperature fluorine substitution on the electrochemical performance of layered $LiNi_{0.8}Co_{0.1}Mn_{0.1}O_{2-z}F_z$ cathode materials, Electrochim. Acta 92 (2013) 1–8.

[32] S.J. Shi, J.P. Tu, Y.J. Mai, Y.Q. Zhang, Y.Y. Tang, X.L. Wang, Structure and electrochemical performance of CaF_2 coated $LiMn_{1/3}Ni_{1/3}Co_{1/3}O_2$ cathode material for Li-ion batteries, Electrochim. Acta 83 (2012) 105–112.

[33] H. Sun, J. Hwang, C. Yoon, A. Heller, C.B. Mullins, Capacity degradation mechanism and cycling stability enhancement of AlF_3-coated nanorod gradient Na $[Ni_{0.65}Co_{0.08}Mn_{0.27}]O_2$ cathode for sodium-ion batteries, ACS Nano 12 (2018) 12912–12922.

[34] J. Xie, A.D. Sendek, E.D. Cubuk, X. Zhang, Z. Lu, Y. Gong, T. Wu, F. Shi, W. Liu, E.J. Reed, Y. Cui, Atomic layer deposition of stable $LiAlF_4$ lithium ion conductive interfacial layer for stable cathode cycling, ACS Nano 11 (2017) 7019–7027.

[35] X. Xiong, D. Ding, Z. Wang, B. Huang, H. Guo, X. Li, Surface modification of $LiNi_{0.8}Co_{0.1}Mn_{0.1}O_2$ with conducting polypyrrole, J. Solid State Electrochem. 18 (2014) 2619–2624.

[36] Y.-K. Sun, S.-T. Myung, M.-H. Kim, J. Prakash, K. Amine, Synthesis and characterization of $Li[(Ni_{0.8}Co_{0.1}Mn_{0.1})_{0.8}(Ni_{0.5}Mn_{0.5})_{0.2}]O_2$ with the microscale Core−Shell structure as the positive electrode material for lithium batteries, J. Am. Chem. Soc. 127 (2005), 13411-1318.

[37] Y.-K. Sun, S.T. Myung, B.C. Park, J. Prakash, I. Belharouak, K. Amine, High-energy cathode material for long-life and safe lithium batteries, Nat. Mater. 8 (2009) 320–324.

[38] P. Hou, H. Zhang, Z. Zi, L. Zhang, X. Xu, Core–shell and concentration-gradient cathodes prepared via Co-precipitation reaction for advanced lithium-ion batteries, J. Chem. Mater. A 5 (2017) 4254–4279.

[39] F. Lin, I.M. Markus, D. Nordlund, T.C. Weng, M.D. Asta, H.L. Xin, M.M. Doeff, Surface reconstruction and chemical evolution of stoichiometric layered cathode materials for lithium-ion batteries, Nat. Commun. 5 (2014) 3529.

[40] Z. Chen, Y. Qin, K. Amine, Y.K. Sun, Role of surface coating on cathode materials for lithium-ion batteries, J. Mater. Chem. 20 (2010) 7606–7612.

[41] Y. Zhang, H. Shi, D. Song, H. Zhang, X. Shi, L. Zhang, Facile synthesis of a novel structured $Li[Ni_{0.66}Co_{0.1}Mn_{0.24}]O_2$ cathode material with improved cycle life and thermal stability via ion diffusion, J. Power Sources 327 (2016) 38–43.

[42] K. Du, C. Hua, C. Tan, Z. Peng, Y. Cao, G. Hu, A high-powered concentration-gradient $Li(Ni_{0.85}Co_{0.12}Mn_{0.03})O_2$ cathode material for lithium ion batteries, J. Power Sources 263 (2014) 203–208.

[43] Y.K. Sun, Z. Chen, H.J. Noh, D.J. Lee, H.G. Jung, Y. Ren, S. Wang, C.S. Yoon, S.T. Myung, K. Amine, Nanostructured high-energy cathode materials for advanced lithium batteries, Nat. Mater. 11 (2012) 942–947.

[44] Y. Cho, P. Oh, J. Cho, A new type of protective surface layer for high-capacity Ni-based cathode materials: nanoscaled surface pillaring layer, Nano Lett. 13 (2013) 1145–1152.

[45] H.-J. Noh, S.-T. Myung, H.-G. Jung, H. Yashiro, K. Amine, Y.-K. Sun, Formation of a continuous solid-solution particle and its application to rechargeable lithium batteries, Adv. Funct. Mater. 23 (2013) 1028–1036.

[46] C. Zhan, T. Wu, J. Lu, K. Amine, Dissolution, migration, and deposition of transition metal ions in Li-ion batteries exemplified by Mn-based cathodes – a critical review, Energy Environ. Sci. 11 (2018) 234–257.

[47] J. Lu, C. Zhan, T. Wu, J. Wen, Y. Lei, A.J. Kropf, H. Wu, D.J. Miller, J.W. Elam, Y.K. Sun, X. Qiu, K. Amine, Effectively suppressing dissolution of manganese from spinel lithium manganate via a nanoscale surface-doping approach, Nat. Commun. 5 (2014) 5693.

[48] Z. Chen, J.R. Dahn, Studies of $LiCoO_2$ coated with metal oxides, Electrochem. Solid State Lett. 6 (2003) A221–A224.

[49] W. Luo, J.R. Dahn, Can Zr be substituted for Co in $Co_{1-z}Zr_z(OH)_2$ and $LiCo_{1-z}Zr_zO_2$? J. Electrochem. Soc. 158 (2011) A110–A114.

[50] H.-H. Sun, A. Manthiram, Impact of microcrack generation and surface degradation on a nickel-rich layered $Li[Ni_{0.9}Co_{0.05}Mn_{0.05}]O_2$ cathode for lithium-ion batteries, Chem. Mater. 29 (2017) 8486–8493.

[51] W. Li, A. Dolocan, P. Oh, H. Celio, S. Park, J. Cho, A. Manthiram, Dynamic behaviour of interphases and its implication on high-energy-density cathode materials in lithium-ion batteries, Nat. Commun. 8 (2017) 14589.

[52] Y. Bi, W. Yang, R. Du, J. Zhou, M. Liu, Y. Liu, D. Wang, Correlation of oxygen non-stoichiometry to the instabilities and electrochemical performance of $LiNi_{0.8}Co_{0.1}Mn_{0.1}O_2$ utilized in lithium ion battery, J. Power Sources 283 (2015) 211–218.

[53] H. Liu, Y. Yang, J. Zhang, Reaction mechanism and kinetics of lithium ion battery cathode material $LiNiO_2$ with CO_2, J. Power Sources 73 (2007) 556–561.

[54] P.M. Bertsch, D.B. Hunter, Applications of synchrotron based X-ray microprobes, Chem. Rev. 101 (2001) 1809–1842.

[55] W.-S. Yoon, M. Balasubramanian, K.Y. Chung, X.-Q. Yang, J. McBreen, C.P. Grey, D.A. Fischer, Investigation of the charge compensation mechanism on the electrochemically Li-ion deintercalated $Li_{1-x}Co_{1/3}Ni_{1/3}Mn_{1/3}O_2$ electrode system by combination of soft and hard X-ray absorption spectroscopy, J. Am. Ceram. Soc. 127 (2005) 17479–17487.

[56] B. Xiao, H. Liu, J. Liu, Q. Sun, B. Wang, K. Kaliyappan, Y. Zhao, M.N. Banis, Y. Liu, R. Li, T.K. Sham, G.A. Botton, M. Cai, X. Sun, Nanoscale manipulation of spinel lithium nickel manganese oxide surface by multisite Ti occupation as high-performance cathode, Adv. Mater. 29 (2017) 1703064.

[57] X. Zhang, Z. Bi, W. He, G. Yang, H. Liu, Y. Yue, Fabricating high-energy quantum dots in ultra-thin $LiFePO_4$ nanosheets using a multifunctional high-energy biomolecule—ATP, Energy Environ. Sci. 7 (2014) 2285–2294.

[58] K. Kleiner, J. Melke, M. Merz, P. Jakes, P. Nagel, S. Schuppler, V. Liebau, H. Ehrenberg, Unraveling the degradation process of $LiNi_{0.8}Co_{0.15}Al_{0.05}O_2$ electrodes in commercial lithium ion batteries by electronic structure investigations, ACS Appl. Mater. Interfaces 7 (2015) 19589–19600.

[59] S.K. Jung, H. Gwon, J. Hong, K.Y. Park, D.H. Seo, H. Kim, J. Hyun, W. Yang, K. Kang, Understanding the degradation mechanisms of $LiNi_{0.5}Co_{0.2}Mn_{0.3}O_2$ cathode material in lithium ion batteries, Adv. Energy Mater. 3 (2013) 1300787.

[60] F. Wu, J. Tian, N. Liu, Y. Lu, Y. Su, J. Wang, R. Chen, X. Ma, L. Bao, S. Chen, Alleviating structural degradation of nickel-rich cathode material by eliminating the surface Fm3m phase, Energy Storage Mater. 8 (2017) 134–140.

[61] E.J. Lee, Z. Chen, H.J. Noh, S.C. Nam, S. Kang, D.H. Kim, K. Amine, Y.K. Sun, Development of microstrain in aged lithium transition metal oxides, Nano Lett. 14 (2014) 4873–4880.

[62] P. Yan, J. Zheng, M. Gu, J. Xiao, J.G. Zhang, C.M. Wang, Intragranular cracking as a critical barrier for high-voltage usage of layer-structured cathode for lithium-ion batteries, Nat. Commun. 8 (2017) 14101.

[63] S. Watanabe, M. Kinoshita, T. Hosokawa, K. Morigaki, K. Nakura, Capacity fading of $LiAl_yNi_{1-x-y}Co_xO_2$ cathode for lithium-ion batteries during accelerated calendar and cycle life tests (effect of depth of discharge in charge–discharge cycling on the suppression of the micro-crack generation of $LiAl_yNi_{1-x-y}Co_xO_2$ particle), J. Power Sources 260 (2014) 50–56.

[64] J. Wang, Y. Yu, B. Li, P. Zhang, J. Huang, F. Wang, S. Zhao, C. Gan, J. Zhao, Thermal synergy effect between $LiNi_{0.5}Co_{0.2}Mn_{0.3}O_2$ and $LiMn_2O_4$ enhances the safety of blended cathode for lithium ion batteries, ACS Appl. Mater. Interfaces 8 (2016) 20147–20156.

[65] D.H. Cho, C.H. Jo, W. Cho, Y.J. Kim, H. Yashiro, Y.K. Sun, S.T. Myung, Effect of residual lithium compounds on layer Ni-rich $Li[Ni_{0.7}Mn_{0.3}]O_2$, J. Electrochem. Soc. 161 (2014) A920–A926.

[66] H. Liu, Y. Yang, J. Zhang, Investigation and improvement on the storage property of $LiNi_{0.8}Co_{0.2}O_2$ as a cathode material for lithium-ion batteries, J. Power Sources 162 (2006) 644–650.